Chemical Science

Accepted Manuscript

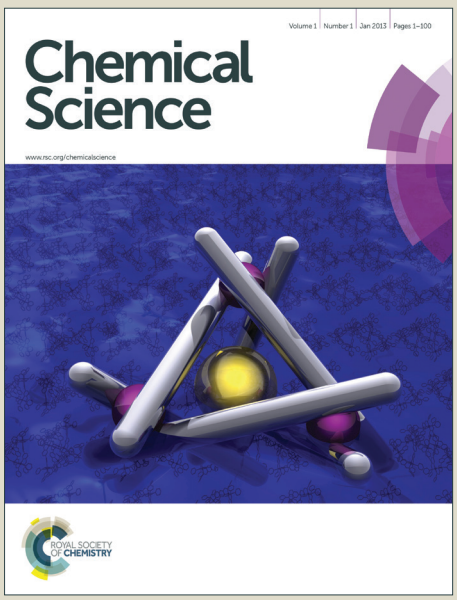

ROYAL SOCIETY OF CHEMISTRY

www.rsc.org/chemicalscience

Hydrogen-Activation Mechanism of [Fe] Hydrogenase Revealed by Multi-Scale Modeling†

Arndt Robert Finkelmann,[a] Hans Martin Senn,[b]* and Markus Reiher[a]*

Received Xth XXXXXXXXXX 20XX, Accepted Xth XXXXXXXXX 20XX
First published on the web Xth XXXXXXXXXX 200X
DOI: 10.1039/b000000x

When investigating the mode of hydrogen activation by [Fe] hydrogenases, not only the chemical reactivity at the active site is of importance but also the large-scale conformational change between the so-called *open* and *closed* conformations, which leads to a special spatial arrangement of substrate and iron cofactor. To study H_2 activation, a complete model of the solvated and cofactor-bound enzyme in complex with the substrate methenyl-H_4MPT$^+$ was constructed. Both the *closed* and *open* conformations were simulated with classical molecular dynamics on the 100 ns time scale. Quantum-mechanics/molecular-mechanics calculations on snapshots then revealed the features of the active site that enable the facile H_2 cleavage. The hydroxyl group of the pyridinol ligand can easily be deprotonated. With the deprotonated hydroxyl group and the structural arrangement in the *closed* conformation, H_2 coordinated to the Fe center is subject to an ionic and orbital push–pull effect and can be rapidly cleaved with a concerted hydride transfer to methenyl-H_4MPT$^+$. An intermediary hydride species is not formed.

1 Introduction

[Fe] hydrogenase[1–5], which features a mononuclear iron complex in the active site, differs in the mode of action compared to [NiFe] and [FeFe] hydrogenases[6–10]. In [FeFe] and [NiFe] hydrogenases, direct H_2 cleavage or formation is a redox process accomplished by oxidation state changes of the active Fe and Ni atoms, respectively[6–10]. The reaction catalyzed by [Fe] hydrogenase,

$$\text{methenyl} - \text{H}_4\text{MPT}^+ + \text{H}_2 \rightleftarrows \text{methylene} - \text{H}_4\text{MPT} + \text{H}^+,$$

is fundamentally different. No oxidation-state change of the active iron could be detected experimentally[11–14]. [Fe] hydrogenase requires the substrate methenyl-H_4MPT$^+$ (see Fig. 1), which acts as the hydride acceptor. The question is therefore why the iron cofactor iron-guanylylpyridinol (FeGP) (Fig. 1) is required for catalysis[11,15] even though it does not seem to be redox-active.

An accurate mechanistic description of the H_2 activation process must thus be able to account for the intriguing role of the metal cofactor. Yang and Hall were the first to investigate the mechanism computationally, using a truncated active-site model in an electrostatic continuum[17]. The first main step of the catalytic cycle is the heterolytic H_2 cleavage, with the proton transferred to either the oxypyridine ligand (deprotonated pyridinol) or the cysteinate ligand, which need to be present in the deprotonated form. The second main step is hydride transfer to methenyl-H_4MPT$^+$[17], which is the rate-limiting step[17]. However, the theoretical description with density-functional-theory (DFT) methods is sensitive to the incorporation of empirical dispersion corrections and the energetics of all elemen-

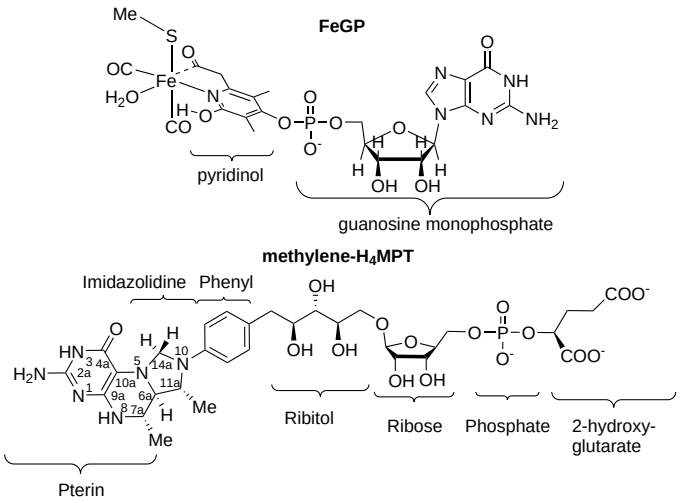

Fig. 1 Top: Lewis structure of the FeGP cofactor. Bottom: Lewis structure of methylene-H_4MPT. The parts of methylene-H_4MPT are denoted according to their chemical building blocks, following Ref. 16. Both molecules are depicted as parametrized for molecular-dynamics simulations (the cysteinate ligand is modeled by a methylthiolate).

† Electronic Supplementary Information (ESI) available: [Computational methodology, additional data]. See DOI: 10.1039/b000000x/

[a] *ETH Zürich, Laboratory of Physical Chemistry, Vladimir-Prelog-Weg 2, Zürich, Switzerland. E-mail: markus.reiher@phys.chem.ethz.ch*
[b] *WestCHEM and School of Chemistry, University of Glasgow, Glasgow G12 8QQ, UK. E-mail: hans.senn@glasgow.ac.uk*

tary reaction steps can be manipulated by first-shell ligand modifications[18]. Yang and Hall formulated the product of H_2 cleavage as a bound dihydrogen species with an elongated, polarized H–H bond, Fe(II)$\cdots H^{\delta-}$—$H^{\delta+}\cdots{}^{-}$O. This species is the resting state in their catalytic cycle[17]. This intermediate could, however, also be described as a hydride complex[18,19].

The difficulties fully to reconcile the experimental observations with that mechanism, which was derived based on a small model, point to the need for an extended theoretical treatment of the reaction. Any mechanistic proposals should be compatible with the following experimental data: (i) If the key intermediate was a stable hydride species, the electronic structure of the Fe atom would change. However, experimental and theoretical Mössbauer spectra indicate that no stable hydride or H_2-bound species exists under turnover conditions[12,19,20]. (ii) Model compounds that accurately mimic the first coordination sphere of the iron do not even bind H_2[21–23], hence, the protein environment is likely to be crucial. (iii) In model compounds, protonating the thiolate ligand leads to dissociation of the ligand[24]. This indicates that also in the enzyme, the thiolate might not be a viable proton acceptor. (iv) Mutating histidine 14 to alanine reduces the catalytic activity to 1 % of the wild-type level[16,25]. The mechanism should thus explain why His14 is important for the catalytic activity.

Already in 2009, Hiromoto *et al.* suggested that a large-scale protein motion might play a role in catalysis[16]. The dimeric protein has three subunits (see Fig. 2): The central subunit, which is formed from the intertwined C-terminal domains of both monomers, and two identical peripheral subunits[26]. The peripheral subunits each harbor an FeGP cofactor[25]; methenyl-H_4MPT^+ binds to the central subunit[16]. The protein can adopt two conformational states, referred to as *open* and *closed*, respectively. In the *open* conformation, there is a cleft between the central and the peripheral subunits, as shown in Fig. 2[25,27].

Hiromoto *et al.* proposed a mechanism where binding of methenyl-H_4MPT^+ to the *open* enzyme induces the transition to the *closed* conformation, in which methenyl-H_4MPT^+ and FeGP are arranged such that H_2 binding and cleavage can occur and methenyl-H_4MPT^+ is reduced to methylene-H_4MPT. Thus, the *closed* enzyme is the reactive conformation. Transition back to the *open* conformation and dissociation of the product methylene-H_4MPT closes the catalytic cycle. Hiromoto *et al.* further postulated that the geometrical arrangement of FeGP and methenyl-H_4MPT^+ imposed by the protein in the *closed* conformation is necessary for catalysis to occur.

To model the reaction accurately, a method is required that incorporates the geometrical constraints imposed by the protein and, if possible, also the electronic polarization exerted by the environment. Combined quantum mechanics/molecular mechanics (QM/MM) fulfils both these requirements[28,29]. A further complication is that a crystal structure of the *closed* conformation is only available for the apoenzyme[26], while the holoenzyme could only be crystallized in the *open* conformation[25,27]. A crystal structure of the enzyme in complex with the substrate is available only for the C176A mutant in the *open* conformation. Thus, suitable starting structures for the wild-type holoenzyme–substrate complex in the *open* and *closed* conformations must be devised first.

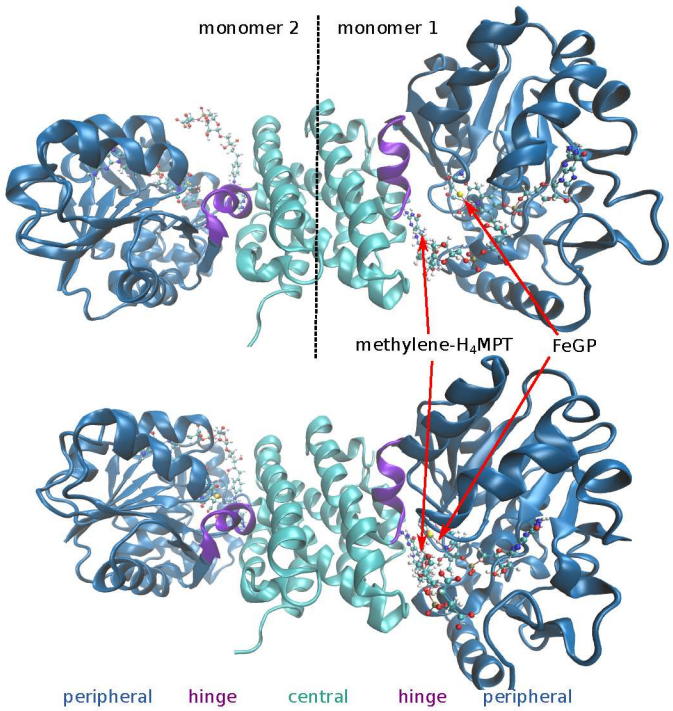

Fig. 2 Cartoon structure of our model of the substrate- and cofactor-bound protein dimer in the *open* conformation (top) and in the *closed* conformation (bottom). The red arrows point to the Fe-center and the hydride-accepting carbon atom of the substrate.

To investigate the crucial H_2 cleavage step, we generated such starting structures of the enzyme–substrate complex in the *open* and *closed* conformations. In the subsequent molecular-dynamics (MD) simulations, the FeGP cofactor and methylene-H_4MPT (compare Fig. 1) were parametrized with the General Amber Force Field (GAFF)[30]. We chose to simulate the enzyme–product complex because methylene-H_4MPT is more straightforward to parameterize with GAFF than methenyl-H_4MPT^+. According to the principle of microscopic reversibility[31], this corresponds to the product structure directly after hydride transfer, and the sampled configurations are relevant for both reaction directions. The Fe atom, both CO ligands, the cysteinate S atom, the acyl CO of the pyridinol ligand, and the oxygen atom of the bound water were positionally restrained to avoid the need for Fe–L bonded parameters. As FeGP is strongly bound to the peripheral sub-

unit, these restraints effectively lock the hinge motion that would interconvert *open* and *closed* conformations. However, this conformational change is likely to take place on a time scale much longer than the sampling times used here. The protein was described with the Amber ff03 force field[32,33]. MD simulations were run with GROMACS 4.5.5[34–37] (*open* conformation: 100 ns, *closed* conformation: 95 ns). Starting from snapshots of the MD trajectory, the H_2 splitting reaction was investigated by QM/MM calculations. These were performed with CHEMSHELL[38–40] interfaced to Turbomole[41,42] as QM back-end. QM calculations used the TPSS-D3[43,44] DFT method with the def2-TZVP[45] basis set for iron and the def2-SVP[46] basis set on all other atoms. The effect of a larger basis set was assessed for one reaction step and the differences in energies and structures were found to be negligible. The TPSS exchange-correlation functional is computationally efficient and reliable[47] and has already been applied in earlier studies of [Fe] hydrogenase[17,18]. Because of the many non-covalent contacts of methylene-H_4MPT and FeGP, the use of dispersion corrections significantly affects the hydride transfer step in smaller models[18], which is the reason for applying the Grimme 'D3' correction here as well[44]. Details on model construction and computational methods can be found in the electronic supporting information (ESI).

Herein, we use a full model of the dimeric enzyme in molecular-dynamics simulations and QM/MM calculations to address two central questions relating to the H_2-activation mechanism in [Fe] hydrogenase. These are the protonation state of the FeGP cofactor and the possible H_2-activation pathways in the *closed* conformation.

2 Molecular dynamics simulations

2.1 *Open* conformation

The MD simulations of the dimer with both monomers in the *open* conformation yield insights into the dynamics around the cofactor in this non-reactive conformation. The methylene-H_4MPT molecules (one bound to each monomer) stay attached to the central subunit of the protein throughout the simulation, mainly due to hydrogen-bonding interactions. Most of these interactions were already identified in the crystal structure[16] and remained largely stable throughout the MD trajectory. Important hydrogen bonds are formed between the 2a-amino group of the pterin unit (see Fig. 3) to the backbone carbonyls of Thr317 and Cys250. The carbonyl group of Cys250 also forms a hydrogen bond with the pterin N3–H. The hydroxyl of Ser320 occasionally forms a hydrogen bond to the pterin 2a-amino group and the carbonyl of Ser320 with the pterin N8–H. The hydroxyl group of Ser254 occasionally also engages in a hydrogen bond to the pterin 2a-amino group. The tail of methylene-H_4MPT is highly flexible and mainly involved in hydrogen bonds to surrounding water molecules. One relatively stable hydrogen bond is formed between Lys151 and either of the glutarate carboxylates (but also to the phosphate). The tail can adopt an extended conformation, and occasionally the glutarate carboxylates form hydrogen bonds with the distant residues Asn153, Lys154, Lys182 or Lys131. However, the predominant conformation of the tail is U-shaped, with the bend at the ribose. Snapshots from the MD simulations with methylene-H_4MPT in either conformation are shown in Fig. 3.

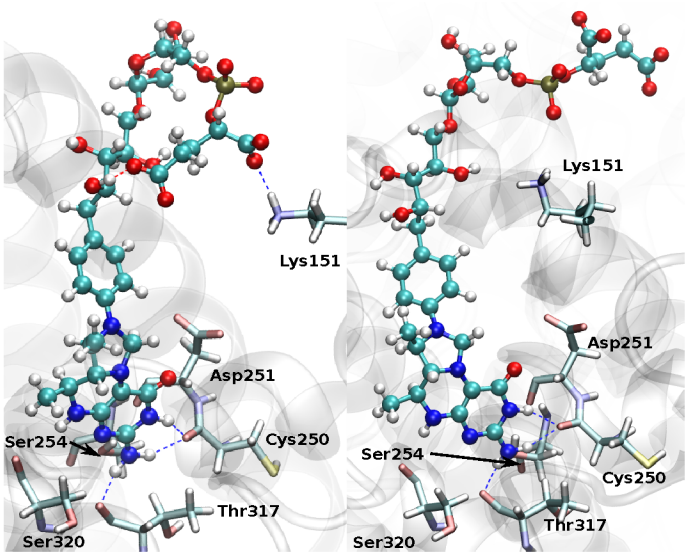

Fig. 3 Representative snapshots of methylene-H_4MPT in the U-shaped conformation (left) and in an extended conformation (right).

The different conformational behavior of the head and tail parts of bound methylene-H_4MPT are mirrored in the RMSD (root-mean-square deviation) with respect to the starting structure. The evolution of the RMSDs of the head and tail parts of both independent methylene-H_4MPT molecules over the whole trajectory are plotted in Fig. 4. The RMSD of the head fluctuates between 1 to 2 Å, so this part of the molecule remains essentially fixed. In contrast, the RMSD of the conformationally flexible, very mobile tail is around 5 Å (U-shaped tail), with values up to 10 Å corresponding to the extended conformation.

In the *open* conformation, the Fe center is exposed to the solvent. The hydroxyl group of the pyridinol ligand mainly hydrogen-bonds to the water molecule coordinated to Fe (whose oxygen atom was positionally restrained). It can also form hydrogen bonds to bulk water molecules. Interestingly, there is a relatively abundant conformation where the hydroxyl group forms a hydrogen bond to His14. His14 is known to be crucial for high catalytic rates, since a H14A mu-

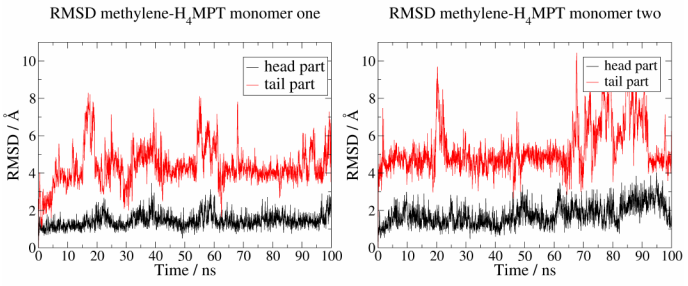

Fig. 4 RMSD evolution of the head and tail parts of methylene-H_4MPT bound to monomer 1 (left panel) and monomer 2 (right panel) during the simulation of the *open* conformation. To calculate the RMSD, one frame was selected every 40 ps and the protein backbone atoms of every structure were aligned.

tation reduces the turnover rate to 1 % of the wild-type level[25]. The presence of this hydrogen-bonded conformation suggests that His14 may act as a base to deprotonate the pyridinol ligand, as previously suggested[16,25]. The distance between the hydroxyl proton and N^{ε} of His14 for both monomers is plotted in Fig. 5. In monomer 1, this hydrogen bond is formed frequently at the beginning of the trajectory but is no longer present beyond 36 ns, whereas in monomer 2, it was mainly observed later during the simulation (see Fig. 5).

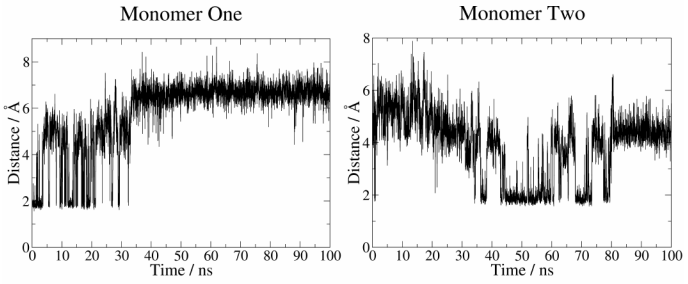

Fig. 5 Distance between the proton of the pyridinol OH group and N^{ε} of His14 for both monomers during the MD simulation of the *open* conformation.

2.2 *Closed* conformation

The simulation of the *closed* conformation samples the conformations of the protein in the state that is believed to be reactive[16]. The reduced substrate methylene-H_4MPT is bound in the active-site cleft with the hydride-accepting C14a atom in spatial proximity to the Fe atom of FeGP. The geometrical arrangement of methylene-H_4MPT and the iron center is stable throughout the simulation. The mean distance between Fe and C14a increased from approximately 3.8 Å (0 to 30 ns) to around 4.3 Å (30 to 90ns) in monomer 1, while it remained constant at approximately 4.3 Å throughout the simulation of monomer 2. Notably, methylene-H_4MPT blocks a water channel identified in the crystal structure[16]. However, a few water molecules are still able to enter the active site by passing along the cofactor already during the first few nanoseconds of the MD simulation. This fast access of a few water molecules indicates that water is able to enter the active-site region through the cavity in the *closed* conformation.

The hydrogen bond between the pyridinol hydroxyl and His14, already observed in the *open* conformation, is formed in the *closed* conformation as well. The distance between the hydroxyl proton and N^{ε} of His14 for both monomers is plotted in Fig. 6. In monomer 2, this hydrogen bond (OH–N^{ε} distance

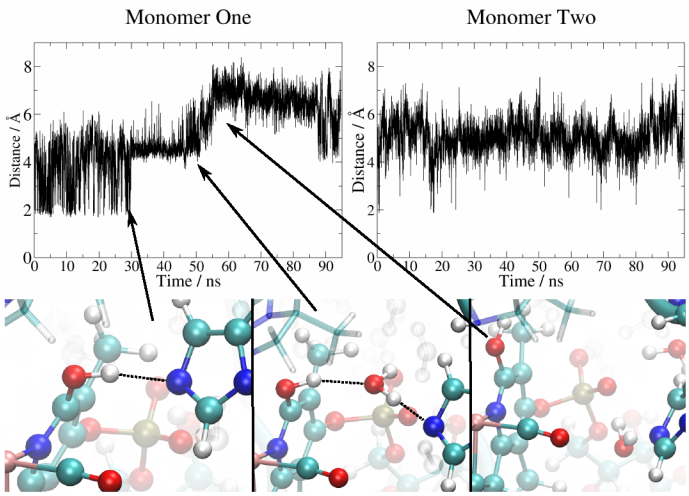

Fig. 6 Top panels: Distance between the proton of the pyridinol OH group and N^{ε} of His14 for both monomers during the MD simulation of the *closed* conformation. Bottom panels: Representative snapshots of the three hydrogen-bonding modes (direct hydrogen bond, one bridging water, no hydrogen bond).

of about 2 Å) is frequently formed and broken over the course of the simulation. In monomer 1, the OH–N^{ε} distance plot shows three stages (see Fig. 6). In the first phase, up to 30 ns, a direct hydrogen bond is often formed. From 30 to 51 ns, the OH–N^{ε} distance remains at around 4.5 Å. In this phase, a water molecule that entered the active site bridges the hydroxyl group and N^{ε} (OH–HOH–N^{ε}). Thus, water-mediated proton transfer should still be possible. In the third phase, from 51 to 88 ns, the hydrogen bond is lost and re-forms again only after 88 ns with one bridging water molecule. Hence, in both monomers, deprotonation of the pyridinol with His14 as the base should be viable. The proton transfer may be mediated by a water molecule bridging between the hydroxyl and the proton-accepting N^{ε}.

3 QM/MM calculations

3.1 Protonation state of the guanylylpyridinol ligand

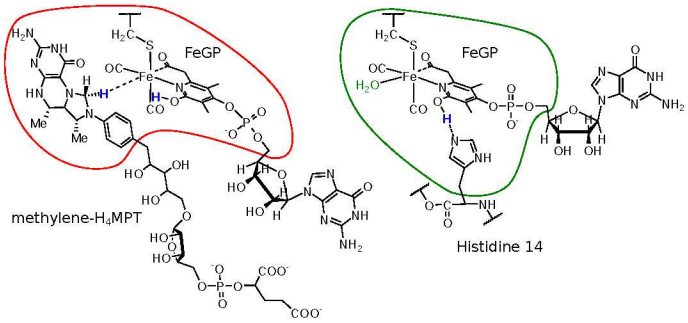

Fig. 7 Left: Lewis representation of the active site of [Fe] hydrogenase with the reduced substrate methylene-H_4MPT. The QM region utilized to model hydrogen splitting is marked in red. Right: Lewis representation of the active site including His14. The QM region chosen to model the proton transfer from pyridinol to His14 (labeling according to PDB code 3H65 [16]) is marked in green. The bound water molecule (green) is only present in the *open* conformation. Hydrogen atoms involved in the reactions are printed blue.

To investigate possible H_2 activation mechanisms, we first need to clarify the protonation state of the active site. The experimentally verified importance of His14 for a high turnover rate [16,25] and the hydrogen bond between His14 and the pyridinol OH observed in the MD simulations point to a crucial role of His14 as the base in the proton transfer pathway. Deprotonation of the hydroxyl group results in a potent proton acceptor (oxypyridine) for heterolytic H_2 cleavage. To investigate the energetics of pyridinol deprotonation, we chose two representative MD snapshots that feature the OH–His14 hydrogen bond: One snapshot from the *open* conformation (at 10.78 ns) and one from the *closed* conformation (at 13.2 ns). Both snapshots were prepared for QM/MM optimization, *i.e.*, the full protein plus a water shell around one of the active sites was extracted (see ESI for details). The QM region contained the FeGP cofactor up to the phosphate linker (with an Fe-bound water in the *open* conformation) and the His14 side chain; see Fig. 7. The optimized structures of the pyridinol/His and oxypridine/$HisH^+$ forms are presented in Fig. 8.

In the *closed* conformation, the proton transfer is endothermic by +2.3 kcal/mol. From a potential-energy surface (PES) scan along the proton-transfer coordinate (defined as the difference between O–H and H–N^{ε} bond lengths), we estimate an upper bound for the proton-transfer barrier of +4.6 kcal/mol (+2.3 kcal/mol for the back reaction). Thus, proton transfer between the pyridinol OH and His14 is facile, with the OH/His form being favoured. Considering that His14 is connected to the bulk solvent through a proton-transfer chain, we conclude

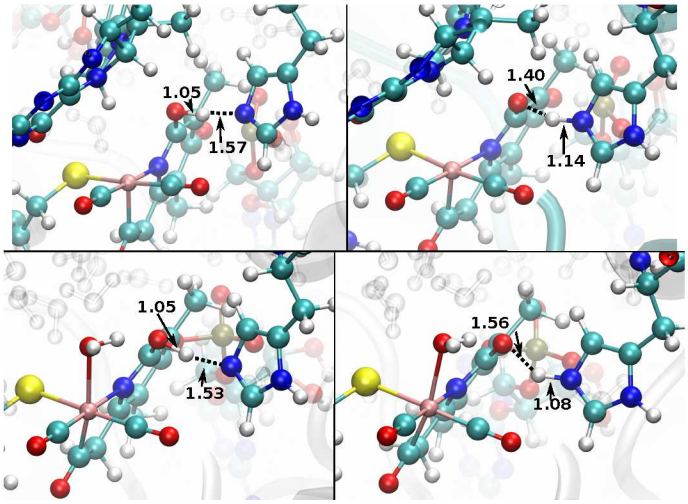

Fig. 8 QM/MM-optimized reactant (left column) and product (right column) structures for the proton transfer from pyridinol OH to His14. Top row: *closed* conformation; bottom row: *open* conformation with Fe-bound water. Water molecules in the active site are shown as "ghost atoms"; selected distances are given in Å.

that the less favoured oxypyridine (O^-/$HisH^+$) form is still present in significant amounts under equilibrium conditions.

In the *open* conformation, the proton transfer is thermoneutral ($\Delta E = 0.0$ kcal/mol). The oxypyridine form is thus equally likely. Although we did not calculate the reaction barrier for this case, it is reasonable to assume that it will be similar to the barrier in the *closed* conformation as the proton transfer reactions are the same in both cases, except for a slight change in the environment. The stabilization of the oxypyridine form in the *open* conformation compared to the *closed* conformation arises because the water molecule coordinated to iron can form a hydrogen bond to the oxypyridine oxygen, stabilizing the anion. Note that the active site in the *open* conformation is exposed to the bulk solvent and thus filled with water (see Fig. 8). For the H_2 activation to proceed, the bound water must be displaced by H_2. Based on all available data, we cannot assess with any certainty if this happens while the enzyme is in the *open* or the *closed* conformation. As we have found that the active site is still accessible to water in the *closed* conformation (see Sect. 2.2), it is certainly possible for H_2 to enter the active site only after the *closed* conformation has formed. What is clear, however, is that the prevailing protonation state of the pyridinol/His14 pair will critically depend on the external pH.

3.2 H_2 activation

To investigate hydrogen cleavage and hydride transfer to methenyl-H_4MPT^+, we chose two representative snapshots

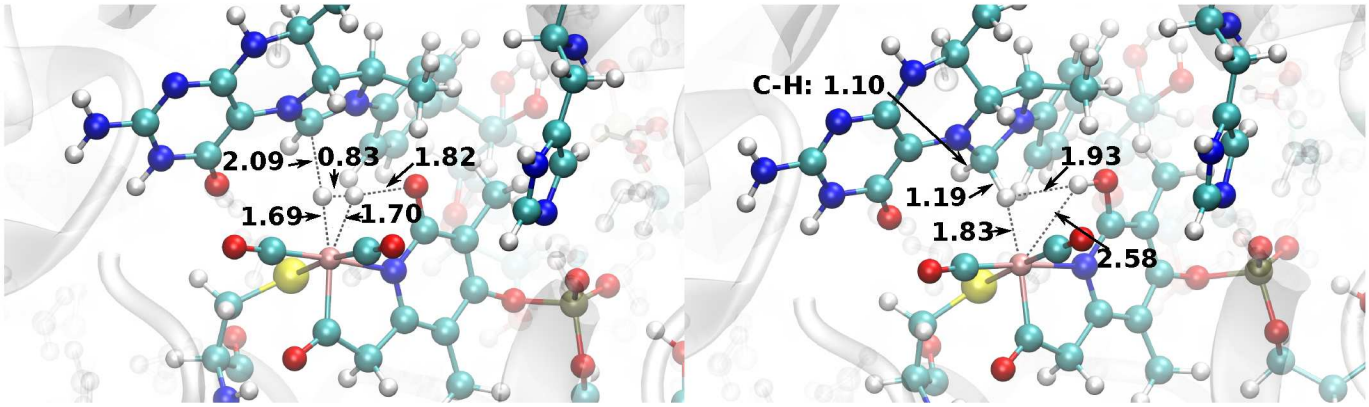

Fig. 9 QM/MM-optimized reactant (left) and product (right) structures of the H_2 cleavage reaction for the scenario with oxypyridine ligand. Distances are given in Å.

from the *closed* conformation: one with a short Fe–C14a distance of 3.7 Å (at 11 ns) and one with a longer distance of 4.3 Å (at 56.5 ns). Because the hydride is transferred to C14a of methenyl-H_4MPT^+, one might expect the reaction to be facilitated by a short Fe–C14a distance, and our discussion thus focuses first on the former snapshot. The QM region included again FeGP up to the phosphate linker, together with the chemically relevant part of the substrate and H_2 (see Fig. 7). In the selected snapshot, the pyridinol-OH–His14 hydrogen bond is not present. Note that His14, in the neutral form, is in the MM region and does not directly participate in the reaction. Considering that the pyridinol–His14 hydrogen bond is frequently formed and broken (see Fig. 6) and that the proton transfer is kinetically facile (see Sect. 3.1), this choice of setup sustains two scenarios: (i) The pyridinol ligand has been deprotonated *via* His14, and the proton removed from the active site through the proton-transfer chain, leaving behind oxypyridine and neutral His14. (ii) The pyridinol ligand remains neutral, without hydrogen-bonding to (also neutral) His14.

3.2.1 H_2 activation *via* oxypyridine. For the scenario with oxypyridine, we studied several possible hydrogen coordination modes to the open coordination site at the Fe center: end-on and two rotamers of side-on coordination. All initial structures converged to a side-on-coordinated hydrogen molecule, which is thus the reactant for the hydrogen cleavage reaction. The structure is shown in Fig. 9. N5 and N10 of the imidazolidine ring are sp^2-hybridized and conjugated with C14a, thus stabilizing the cation. The coordinated H_2 is activated, its bond being elongated to 0.83 Å (from 0.74 Å in free H_2). There is only one reasonable pathway to cleave H_2 in this configuration: In a concerted heterolytic cleavage step, the proton is transferred to the oxypyridine oxygen and the hydride to C14a of methenyl-H_4MPT^+. This reaction is exothermic by −18.7 kcal/mol. A PES scan (along the difference of O–H and H–H bond lengths) provided an upper bound for the barrier of about +1.0 kcal/mol. Despite various attempts, we were unable to locate a stable minimum on the PES that would correspond to an iron hydride species. Hence, we find that the iron is involved in H_2 binding and activation, but does not bind a hydride species. The H_2 cleavage mechanism we have identified here thus complies with the first of the requirements formulated in Sect. 1.

In the reactant complex, the coordinated H_2 is subjected to an electronic push–pull effect from the negatively charged oxypyridine oxygen and the positively charged carbocation of methenyl-H_4MPT^+. This is reflected in the relevant frontier orbitals (Fig. 10): The LUMO has a strong contribution from the p_z orbital on C14a, which is oriented perpendicular to the ring plane. The HOMO−2 is delocalized over the oxypyridine ring and the thiolate S atom, with a strong contribution from the oxypyridine oxygen. (Note that HOMO and HOMO−1 are strongly localized on the phosphate linker and thus do not contribute to the reactivity at the iron center).

In the optimized product structure the O–H bond of the pyridinol hydroxyl points towards the empty coordination site of the iron center (Fig. 9). The newly formed C14a–H bond is pointing towards the Fe atom. It is slightly elongated (1.19 Å compared to 1.10 Å for the other C14a–H bond), indicating a weak interaction with the iron center. Another conformer, where the O–H bond has turned away from the iron, was found to be 2.3 kcal/mol more stable. In both conformers, the imidazolidine ring of methylene-H_4MPT is only slightly puckered. The geometry at N10 is almost planar in both conformers, indicating sp^2 hybridization ($\Delta = 0.02$ Å and $\Delta = 0.10$ Å, respectively; Δ, as defined by Dunitz and co-workers[48], measures the degree of pyramidalization as the distance of the N atom from the plane spanned by its three bonding partners). N5 is planar in the first conformer ($\Delta = 0.00$ Å) and only slightly

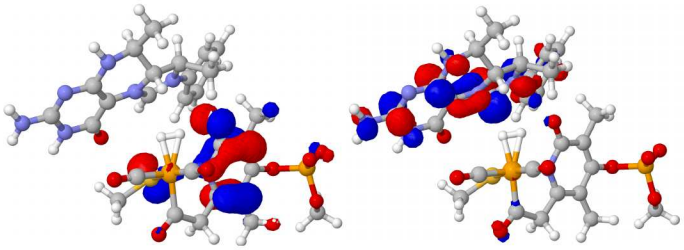

Fig. 10 HOMO−2 (right) and LUMO (left) of the H_2 adduct of the oxypyridine form of the FeGP cofactor.

pyramidalized in the second ($\Delta = 0.21$ Å). The N5 lone pair in the second conformer is synclinal to the C–H^{pro-R} bond. We therefore see no evidence for a beneficial stereoelectronic effect of the nitrogen lone pairs on C–H bond formation, which would require a lone pair to be antiperiplanar to the C–H^{pro-R} bond[49].

Similar results were obtained for the second snapshot, where the substrate was positioned slightly further away from the iron center (4.3 *vs.* 3.7 Å). The cleavage reaction in that case is even more exothermic (by −26.3 kcal/mol, compared to −18.7 kcal/mol for the first snapshot), and again no iron hydride species could be optimized. In the product structure, imidazolidine N5 is sp^3-hybridized ($\Delta = 0.46$ Å, lone pair synclinal to C–H^{pro-R}) while N10 remains again sp^2 ($\Delta = 0.05$ Å) hybridized. We thus find that fluctuations of the substrate position of the order as they were observed in the MD simulations have only a minor effect on the reactivity of [Fe] hydrogenase in the H_2 cleavage step.

3.2.2 H_2 activation *via* thiolate. In the second scenario, we consider the cleavage reaction with a neutral pyridinol ligand. There are two relevant reactant conformers, which differ in the orientation of the pyridinol O–H bond (Fig. 11). In the following, we quote energies relative to the favoured conformer with the O–H pointing away from the iron. The second conformer, where the O–H is pointing towards the coordinated H_2, is 5.7 kcal/mol less stable. Direct H_2 splitting in the favoured conformer, with the pyridinol OH acting as the proton acceptor, is not possible: Product-like starting structures, with one hydrogen atom already transferred to C14a of methenyl-H_4MPT^+, are not stable minima but converged back to reactant structures during optimization. For the second conformer, this pathway is precluded in the first place by the orientation of the pyridinol OH bond.

However, we find for both reactant conformers that hydrogen cleavage can occur with the thiolate ligand, rather pyridinol OH, as the proton acceptor. When the OH group is oriented away from the Fe center, the resulting iron hydride structure is not stable but the hydride is directly transferred to methenyl-H_4MPT^+ to form the product. This reaction is exothermic by −4.4 kcal/mol, significantly less so than hydride cleavage to oxypyridine-O^-. For the reactant conformer with the OH bond oriented towards the Fe center, a stable iron hydride intermediate could indeed be located (Fig. 11). It is only +0.3 kcal/mol higher in energy than the favoured reactant conformer. The hydride Fe–H bond length is 1.61 Å, in excellent agreement with Fe–H bonds in comparable hydride complexes optimized *in vacuo*[19] (1.60 Å). OH rotation, which is likely to have a low activation barrier, triggers the transfer of the hydride from iron to methenyl-H_4MPT^+, yielding the same product as direct H_2 splitting from the preferred conformer (see Fig. 11). The thiolate is thus able to act as the base, which may provide an explanation for the 1 % remaining activity of the H14A mutation[16,25].

Remarkably, the Fe–SH bond in the product (2.34 Å) is even slightly shorter than the Fe–S^- bond in the reactant (2.36 Å). In the product, the thiol proton forms a short hydrogen bond (1.37 Å) to the pterin carbonyl group of methylene-H_4MPT (see Fig. 11), which is a very good hydrogen-bond acceptor because of its conjugation with the guanidine moiety in the pterin ring. This in turn weakens the S–H bond (elongated to 1.51 Å, compared to 1.39 Å in the hydride intermediate), which may be described as "partial deprotonation" of the thiol. The formal thiol ligand in the product is similar in character to a thiolate in terms of its interaction with the metal center. The thiol–pterin hydrogen bond thus makes the thiolate a better proton acceptor in the H_2 splitting step, stabilizes the thiol product, and also makes the thiol a better ligand, preventing it from dissociating like in model complexes. The hydrogen bond is enabled by the exact positioning of the FeGP cofactor and the methenyl-H_4MPT^+ substrate in the active site. As water molecules are still able to access the active site in the *closed* conformation (see Sect. 2.2), we can envisage that the excess proton on the thiol ligand is removed from the active site *via* water.

4 Discussion and Conclusions

[FeFe] and [NiFe] hydrogenases cleave or form H_2 by redox chemistry[7–9]; a basic group close to the active iron atom in [FeFe] hydrogenases is important to donate or accept protons. The mechanism of hydrogen activation in [Fe] hydrogenase is different. The enzyme has two large-scale conformations, which differ in the relative orientation of the central and peripheral subunits. In the *closed* conformation, the mononuclear iron cofactor (FeGP) and the substrate are kept in close proximity in an arrangement that is stable over longer time scales, as we have shown by MD simulations. Our QM/MM calculations have demonstrated that the pyridinol hydroxyl group can easily be deprotonated *via* His14 to form the oxypyridine ligand. The pyridinol ligand in [Fe] hydrogenase thus has a function similar to the bridgehead amine

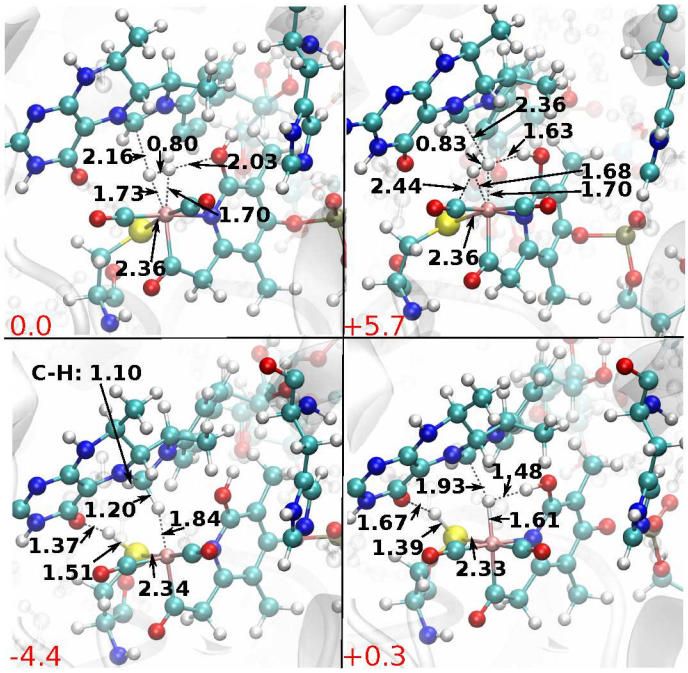

Fig. 11 Top row: Structures of the H_2 adduct for the second scenario with neutral pyridinol; the pyridinol OH can be oriented away from Fe (top left) or towards Fe (top right). Bottom row: Products of H_2 cleavage, with the proton transferred to the thiolate; with the hydroxyl oriented away from Fe (bottom left) and towards Fe (bottom right). Distances are given in Å; relative energies with respect to the favoured adduct are indicated in red in kcal/mol .

group of the H-cluster in [FeFe] hydrogenases[50]. However, the oxypyridine plays an additional, crucial role in activating H_2: It is close to the iron atom and represents an ideal Lewis base. On the other side of the iron is the carbocationic C14a of the substrate methenyl-H_4MPT$^+$, which is an ideal Lewis acid. Furthermore, both groups are ionic. When a hydrogen molecule coordinates to the iron, it is polarized by these charges and subjected to an electronic push–pull effect exerted by the Lewis pair. The spatial arrangement in the *closed* conformation is exactly such that the coordinated H_2 lies in-between C14a$^+$ and O$^-$. This leads to facile, exothermic heterolytic H_2 cleavage, without involving electron transfers to/from the metal center. The role of oxypyridine as a Lewis base was also proposed to be relevant for the inhibition by isocyanides[51]. The Lewis acid C14a$^+$ is only present in proximity to FeGP when methenyl-H_4MPT$^+$ is bound in the *closed* conformation. H_2 cleavage in the *open* conformation is thus unlikely.

It should be noted that our findings are based on only one or two snapshots for each scenario. However, as the barriers are very low, it is unlikely that the consideration of additional snapshots would lead to qualitatively different conclusions. Furthermore, we considered the proton transfer from pyridinol to His14 and H_2 cleavage (with neutral His14) as separate steps. Other scenarios are conceivable, for instance, with His14 remaining protonated during H_2 cleavage or a proton transfer from pyridinol to His14 concerted with H_2 cleavage (direct His14 involvement). The facile pyridinol deprotonation reaction suggests that such a direct involvement of His14 in the H_2 cleavage step (general base effect) might be possible.

The activation mechanism we have described is reminiscent of hydrogen activation by frustrated Lewis pairs[52]. The hydrogen-bound adduct does not need to be very stable since the H_2 cleavage barrier is extremely low (about 1 kcal/mol). Hence, any H_2 binding event can directly lead to H_2 cleavage, without requiring a long-lived H_2-bound intermediate.

When the pyridinol ligand is not deprotonated, it is still possible to split H_2 *via* proton transfer to the thiolate ligand. However, we have found this pathway to be much less favorable. This is consistent with observations in biomimetic model complexes that thiol is a poor ligand[24]. The pyridinol/oxypyridine equilibrium must be strongly affected by the pH, so we would expect the reactivity to depend critically on pH as well, which is indeed the case[1,53].

The overall rate of the enzyme depends on additional factors. For the hydrogen activation mechanism, the reactive *closed* conformation must be formed, which requires large-scale protein motions. Since the reaction barriers in the *closed* conformation are very small, we can only speculate that the change in free energy from *open* to *closed* conformation and the associated free-energy barrier might be rate-limiting for the overall enzymes activity.

The atomistic mechanism of H_2 activation in [Fe] hydrogenase we have proposed herein satisfies the criteria set out in Sect. 1: No stable hydride intermediate; no occurrence of, or requirement for, a long-lived H_2 adduct; no involvement of the thiolate ligand as a proton acceptor; a crucial role for His14. In our preferred mechanism, the pyridinol hydroxyl group and His14, together with the stable placement of the substrate carbocation in the active site, are the essential players, which is in accord with the observation that the enzyme loses 99 % of its activity upon H14A mutation[25]. The residual activity of the H14A mutant can be explained by the alternative, less favorable activation pathway *via* the thiolate.

In the *open* conformation, which might be prevailing in solution, the water-bound FeGP cofactor is the most probable form, which agrees with the results of a theoretical Mössbauer study[19].

References

1 B. Schwörer, V. M. Fernandez, C. Zirngibl and R. K. Thauer, *Eur. J. Biochem.*, 1993, **212**, 255–261.

2 A. R. Klein, G. C. Hartmann and R. K. Thauer, *Eur. J. Biochem.*, 1995, **233**, 372–376.

3 G. C. Hartmann, E. Santamaria, V. M. Fernández and R. K. Thauer, *J. Biol. Inorg. Chem.*, 1996, **1**, 446–450.
4 C. Zirngibl, W. van Dongen, B. Schwörer, R. von Bünau, M. Richter, A. Klein and R. K. Thauer, *Eur. J. Biochem.*, 1992, **208**, 511–520.
5 M. J. Corr and J. A. Murphy, *Chem. Soc. Rev.*, 2011, **40**, 2279–2292.
6 W. Lubitz, H. Ogata, O. Rüdiger and E. Reijerse, *Chem. Rev.*, 2014, **114**, 4081–4148.
7 K. A. Vincent, A. Parker and F. A. Armstrong, *Chem. Rev.*, 2007, **107**, 4366–4413.
8 J. C. Fontecilla-Camps, A. Volbeda, C. Cavazza and Y. Nicolet, *Chem. Rev.*, 2007, **107**, 4273–4303.
9 W. Lubitz, E. Reijerse and M. van Gastel, *Chem. Rev.*, 2007, **107**, 4331–4365.
10 A. L. De Lacey, V. M. Fernández, M. Rousset and R. Cammack, *Chem. Rev.*, 2007, **107**, 4304–4330.
11 E. J. Lyon, S. Shima, G. Buurman, S. Chowdhuri, A. Batschauer, K. Steinbach and R. K. Thauer, *Eur. J. Biochem.*, 2004, **271**, 195–204.
12 S. Shima, E. J. Lyon, R. K. Thauer, B. Mienert and E. Bill, *J. Am. Chem. Soc.*, 2005, **127**, 10430–10435.
13 X. Wang, Z. Li, X. Zeng, Q. Luo, D. J. Evans, C. J. Pickett and X. Liu, *Chem. Commun.*, 2008, **30**, 3555–3557.
14 M. Salomone-Stagni, F. Stellato, C. M. Whaley, S. Vogt, S. Morante, S. Shima, T. B. Rauchfuss and W. Meyer-Klaucke, *Dalton Trans.*, 2010, **39**, 3057–3064.
15 E. J. Lyon, S. Shima, R. Boecher, R. K. Thauer, F.-W. Grevels, E. Bill, W. Roseboom and S. P. Albracht, *J. Am. Chem. Soc.*, 2004, **126**, 14239–14248.
16 T. Hiromoto, E. Warkentin, J. Moll, U. Ermler and S. Shima, *Angew. Chem. Int. Ed.*, 2009, **48**, 6457–6460.
17 X. Yang and M. B. Hall, *J. Am. Chem. Soc.*, 2009, **131**, 10901–10908.
18 A. R. Finkelmann, M. T. Stiebritz and M. Reiher, *J. Phys. Chem. B*, 2013, **117**, 4806–4817.
19 J. Gubler, A. R. Finkelmann and M. Reiher, *Inorg. Chem.*, 2013, **52**, 14205–14215.
20 E. D. Hedegård, S. Knecht, U. Ryde, J. Kongsted and T. Saue, *Phys. Chem. Chem. Phys.*, 2014.
21 D. Chen, R. Scopelliti and X. Hu, *Angew. Chem. Int. Ed.*, 2011, **50**, 5671–5673.
22 D. Chen, A. Ahrens-Botzong, V. Schünemann, R. Scopelliti and X. Hu, *Inorg. Chem.*, 2011, **50**, 5249–5257.
23 D. Chen, R. Scopelliti and X. Hu, *Angew. Chem. Int. Ed.*, 2010, **49**, 7512–7515.
24 D. Chen, R. Scopelliti and X. Hu, *Angew. Chem.*, 2012, **51**, 1955–1957.
25 S. Shima, O. Pilak, S. Vogt, M. Schick, M. S. Stagni, W. Meyer-Klaucke, E. Warkentin, R. K. Thauer and U. Ermler, *Science*, 2008, **321**, 572–575.
26 O. Pilak, B. Mamat, S. Vogt, C. H. Hagemeier, R. K. Thauer, S. Shima, C. Vonrhein, E. Warkentin and U. Ermler, *J. Mol. Biol.*, 2006, **358**, 798–809.
27 T. Hiromoto, K. Ataka, O. Pilak, S. Vogt, M. S. Stagni, W. Meyer-Klaucke, E. Warkentin, R. K. Thauer, S. Shima and U. Ermler, *FEBS Lett.*, 2009, **583**, 585–590.
28 A. Warshel and M. Levitt, *J. Mol. Biol.*, 1976, **103**, 227–249.
29 H. M. Senn and W. Thiel, *Angew. Chem. Int. Ed.*, 2009, **48**, 1198–1229.
30 J. Wang, R. M. Wolf, J. W. Caldwell, P. A. Kollman and D. A. Case, *J. Comput. Chem.*, 2004, **25**, 1157–1174.
31 R. C. Tolman, *The principles of statistical mechanics*, Oxford University Press: London, UK, 1938.
32 Y. Duan, C. Wu, S. Chowdhury, M. C. Lee, G. Xiong, W. Zhang, R. Yang, P. Cieplak, R. Luo, T. Lee, J. Caldwell, J. Wang and P. Kollman, *J. Comput. Chem.*, 2003, **24**, 1999–2012.
33 M. C. Lee and Y. Duan, *Proteins*, 2004, **55**, 620–634.
34 H. J. C. Berendsen, D. van der Spoel and R. van Drunen, *Comput. Phys. Commun.*, 1995, **91**, 43–56.
35 D. Van Der Spoel, E. Lindahl, B. Hess, G. Groenhof, A. E. Mark and H. J. C. Berendsen, *J. Comput. Chem.*, 2005, **26**, 1701–1718.
36 B. Hess, C. Kutzner, D. van der Spoel and E. Lindahl, *J. Chem. Theor. Comput.*, 2008, **4**, 435–447.
37 S. Pronk, S. Pll, R. Schulz, P. Larsson, P. Bjelkmar, R. Apostolov, M. R. Shirts, J. C. Smith, P. M. Kasson, D. van der Spoel, B. Hess and E. Lindahl, *Bioinformatics*, 2013, **29**, 845–854.
38 *ChemShell, a Computational Chemistry Shell*, see www.chemshell.org.
39 P. Sherwood, A. H. de Vries, M. F. Guest, G. Schreckenbach, C. A. Catlow, S. A. French, A. A. Sokol, S. T. Bromley, W. Thiel, A. J. Turner, S. Billeter, F. Terstegen, S. Thiel, J. Kendrick, S. C. Rogers, J. Casci, M. Watson, F. King, E. Karlsen, M. Sjøvoll, A. Fahmi, A. Schäfer and C. Lennartz, *Theochem*, 2003, **632**, 1–28.
40 S. Metz, J. Kästner, A. A. Sokol, T. W. Keal and P. Sherwood, *WIRS Comput. Mol. Sci.*, 2014, **4**, 101–110.
41 R. Ahlrichs, M. Bär, M. Häser, H. Horn and C. Kölmel, *Chem. Phys. Lett.*, 1989, **162**, 165–169.
42 *TURBOMOLE V6.5 2013, a development of University of Karlsruhe and Forschungszentrum Karlsruhe GmbH, 1989-2007, TURBOMOLE GmbH, since 2007; available from* `http://www.turbomole.com`.
43 J. Tao, J. P. Perdew, V. N. Staroverov and G. E. Scuseria, *Phys. Rev. Lett.*, 2003, **91**, 146401.
44 S. Grimme, J. Antony, S. Ehrlich and H. Krieg, *J. Chem. Phys.*, 2010, **132**, 154104.
45 F. Weigend and R. Ahlrichs, *Phys. Chem. Chem. Phys.*, 2005, **7**, 3297–3305.
46 A. Schäfer, H. Horn and R. Ahlrichs, *J. Chem. Phys.*, 1992, **97**, 2571.
47 T. Weymuth, E. P. A. Couzijn, P. Chen and M. Reiher, *J. Chem. Theory Comput.*, 2014, DOI:10.1021/ct500248h.
48 K. L. Brown, L. Damm, J. D. Dunitz, A. Eschenmoser, R. Hobi and C. Kratky, *Helv. Chim. Acta*, 1978, **61**, 3108–3135.
49 S. Bartoschek, G. Buurman, R. K. Thauer, B. H. Geierstanger, J. P. Weyrauch, C. Griesinger, M. Nilges, M. C. Hutter and V. Helms, *ChemBioChem*, 2001, **2**, 530–541.
50 H.-J. Fan and M. B. Hall, *J. Am. Chem. Soc.*, 2001, **123**, 3828–3829.
51 H. Tamura, M. Salomone-Stagni, T. Fujishiro, E. Warkentin, W. Meyer-Klaucke, U. Ermler and S. Shima, *Angew. Chem. Int. Ed.*, 2013, **52**, 9656–9659.
52 D. W. Stephan and G. Erker, *Angew. Chem. Int. Ed.*, 2010, **49**, 46–76.
53 C. Zirngibl, R. Hedderich and R. K. Thauer, *FEBS Lett.*, 1990, **261**, 112–116.